Int. J. Nanosci. Nanotechnol., Vol. 8, No. 3, Sep. 2012, pp. 149-156

Lead Selenide Nanomaterials: Hydrothermal Synthesis, Characterization, Optical Properties and DFT Calculations

M. Hatami[1], M. H. Majles Ara[2*], A. Rostami[3,4], M. Dolatyari[3], M. Mahmudi[3], H. Baghban[3], H. Rasooli[3], M. Afsare[2]

1- Plasma Physics Research Center, Science and Research Branch, Islamic Azad University, Tehran, I. R. Iran.
2- Photonics Lab., Kharazmi University, Tehran, I. R. Iran.
3- School of Engineering-Emerging Technologies, University of Tabriz, Tabriz, I. R. Iran.
4- Photonics and Nanocrystal Research Lab. (PNRL), Faculty of Electrical and Computer Engineering, University of Tabriz, Tabriz, I. R. Iran

(*) Corresponding author: majlesara@gmail.com
(Received:10 Feb. 2012 and Accepted: 20 June 2012)

Abstract:
Well-defined crystalline PbSe nanocubes and nanospheres have been synthesized through a simple hydrothermal method by using Pb^{2+}- EDTA and Pb^{2+}- oleylamine complexes at 180°C for different reaction times. Composition and morphology of the samples have been characterized by means of XRD and SEM. Gradual release process of Pb^{2+} from Pb^{2+}-EDTA and Pb^{2+}-oleylamine complexes can adjust the growth rate. Both EDTA and oleylamine play important roles in the crystal growth of PbSe nanomaterials. The electronic band structure along with density of states (DOS) calculated by the DFT method indicates that PbSe have a direct energy band gap of 0.51 eV. The optical properties, including the dielectric and absorption of the compounds are calculated by DFT method and analyzed based on the electronic structures. Two absorption bands have been observed in the absorption spectra identified from density of state (DOS) calculations.
Keywords: *nanostructures, Lead selenide, optical properties, DFT calculations.*

1. INTRODUCTION

The IV–VI semiconductors PbS, PbSe and PbTe with the cubic NaCl (rock salt) structure, generally known as lead salts, have been the subject of a vast amount of theoretical and experimental work during the past decades, motivated not only by their technological applications, but also by their unusual physical properties [1]. Lead salts are narrow-gap semiconductor compounds with strong ionic characteristics. The unusual characteristics of lead salts, such as the positive temperature coefficient of the gap ($dE/dT > 0$) [2], the high static dielectric constant [3], and the large carrier mobility [4], make them unique among polar compounds and offer important applications in many fields, such as infrared detectors, light-emitting devices, and more recently as infrared lasers in fiber optics, thermoelectric materials, solar energy panels and window coatings [5–8].

Over the past few years, various methods, including surfactant aided solid-state reaction, microbial synthesis, sonochemical, electro-deposition and microwave irradiation, radiation, photochemical, solution-based, hydrothermal, solvothermal route, pulse sonoelectrochemical technique, and so on [9–14], have been employed to synthesize PbSe nanostructures with various morphologies, such

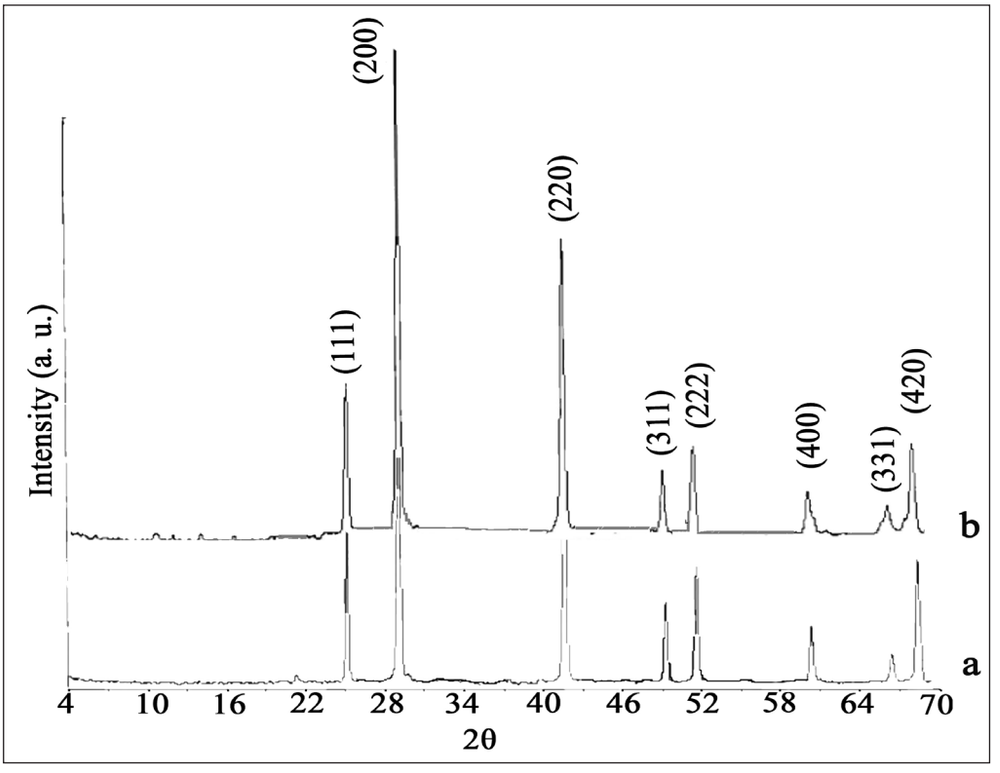

Figure 1: *XRD patterns of cubic and spherical structured PbSe grown at 180 °C for 24 h synthesized by a) EDTA and b) Oleylamine.*

as nanorods, nano-tubes, nano-wires, nano-rings, nano-tubes, and other nanocrystals [15–24].

Developing novel and simple methods to synthesize material at the nanometer scale is of considerable interest where the most straightforward method to synthesize metal selenide is by a direct combination of elemental metal and selenium powder at a relatively low temperature. Most of the shape-controlled preparation of PbSe has been made with the assistance of surfactants. However, surfactant-free methods are less touched area until now. It is well-known that the hydrothermal synthesis is an environmental friendly method for the preparation of materials since the reactions are carried out in a sealed container.

Herein, we report a facile one-step hydrothermal route for the synthesis of high-quality cubic and spherical PbSe at relatively low temperature (180°C). Under such conditions, toxic solvents such as ethylenediamine, pyridine and benzene can be avoided. Cubic PbSe have been obtained in distilled water or an alkaline water solution with the assistance of EDTA as shape controller. In the synthesis of spherical PbSe oleylamine was used instead of EDTA. To the best of our knowledge, there is no report on synthesis of PbSe nanoparticles by this method.

Several *ab initio* calculations [25–30] have been performed to study the structural and electronic properties of PbSe. We will present a systematic study of the electronic and optical properties of the boehmite through the density functional theory calculations using CASTEP code.

2. RESULTS AND DISCUSSION

2.1. Powder X-ray diffraction (XRD)

A typical XRD pattern of the obtained sample is shown in Figure 1, which was synthesized at 180 °C for 24 h in water solution. The XRD pattern shows all Bragg's reflection for (1 1 1), (2 0 0), (2 2 0), (3

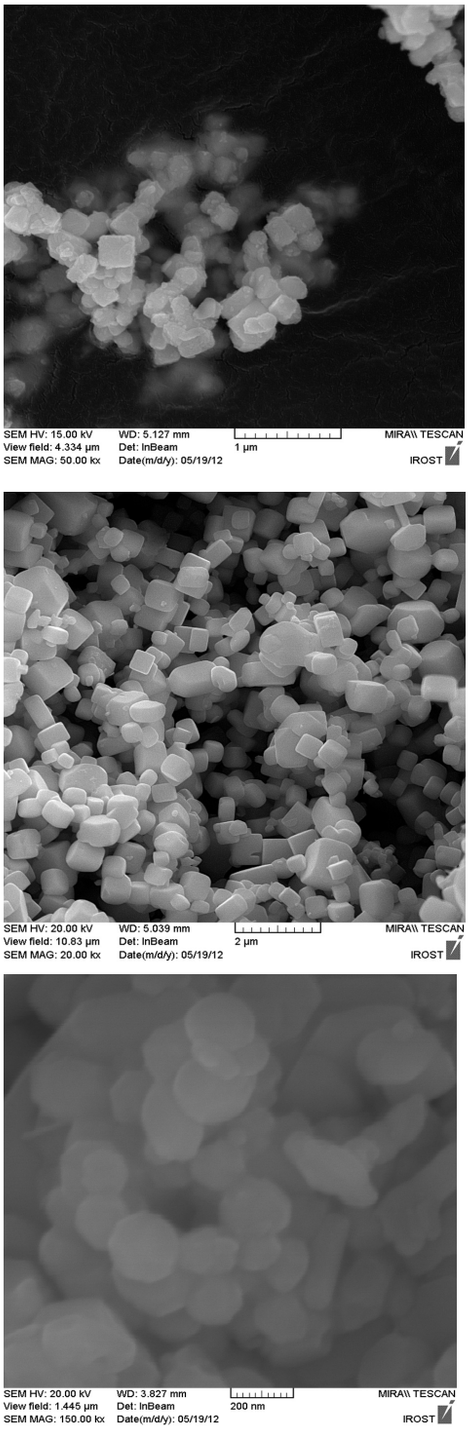

Figure 2: *SEM images of synthesized PbSe (a) with EDTA at 180 °C for 24 h (b) with EDTA at 180 °C for 48 h and (c) with oleylamin at180 °C for 24 h.*

1 1), (2 2 2), (4 0 0), (3 3 1), (4 2 0) and (4 2 2) (h k l) planes. All the diffraction peaks can be readily indexed as the cubic structure PbSe, which agree with the literature datum (PDF No.65-2941). The strong and sharp reflection peaks suggest that the products are highly crystalline. Also, these patterns confirm that PbSe crystallites could be formed with high purity. The broadening of the peaks for PbSe nano-spheres synthesized by oleylamine indicates small size of the synthesized materials.

2.2. Morphology studies

Figures 2 (a) and (b) show SEM images of the mono-dispersed PbSe nano-cubes synthesized at 180°C for 24 and 48 h. The PbSe nano-cubes are uniform in size and most nano-cubes exhibit a glazed and flat surface along with regular shape. Higher magnification also indicates the perfection of the nano-cubes.

Because of the cubic symmetry of PbSe, they prefer to grow into a cubic shape once a particle grows to a certain minimum size when there are no constraints. As shown in Figure 2b, with increasing the reaction time, solid cubes grow larger (average size of cubes for 24 h and 48 h reaction time is 300nm and 500nm, respectively). When oleylamine was used as capping material (instead of EDTA), no cubic particles were observed as shown in Figure 2c. This condition essentially reduces the size of the micelles and nano-spheres are observed (The average size of spheres is about 170nm). This implies the important role of capping materials to form different morphology. On the basis of these observations and a large number of other experiments, we propose a growth mechanism of such nano and micro-structures. Since the reaction of EDTA with Pb^{2+} results in strong bonds, we observed nano-cubes due to stabilization effect and the preferred growth of PbSe in cubic symmetry seeded by the reduced lead. As a result, the existence and gradual release of Pb^{2+} are the key procedure to the growth of PbSe nanocrystal. It is noteworthy to mention that Pb^{2+}-EDTA is a coordination compound, where EDTA serves as ligand, capable of releasing Pb^{2+} gradually. This is a favorable effect for crystal slow growth rate. In the reaction of the Pb^{2+} with oleylamine, the PbSe molecules first grow to the critical size determined

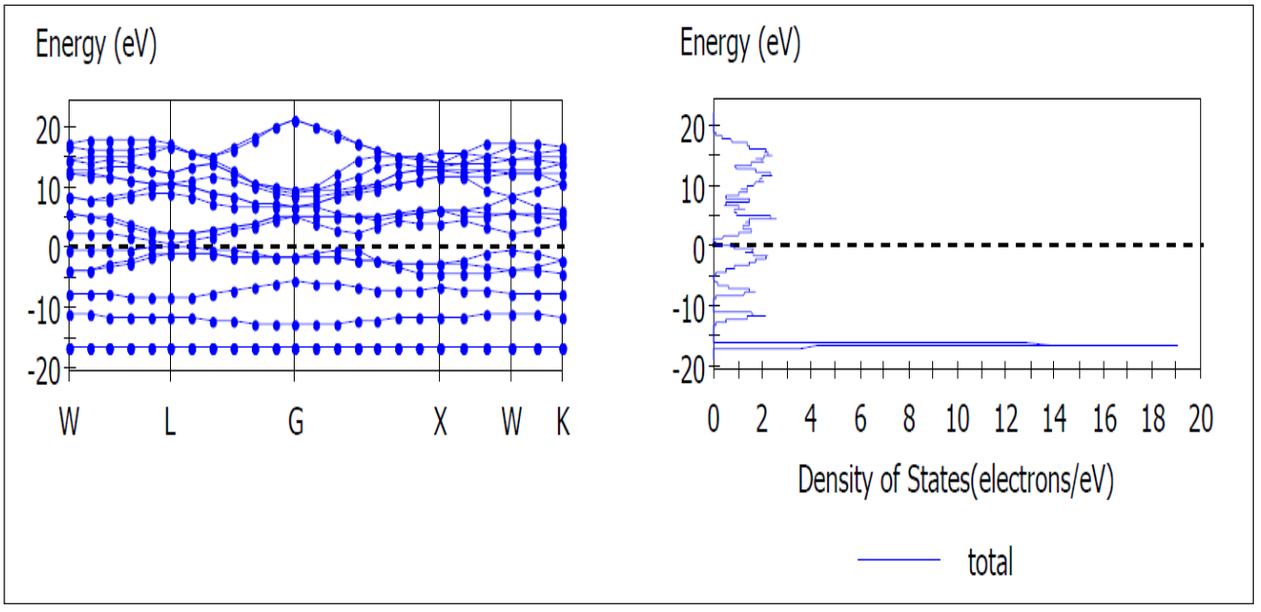

Figure 3: *Calculated band structure for PbSe.*

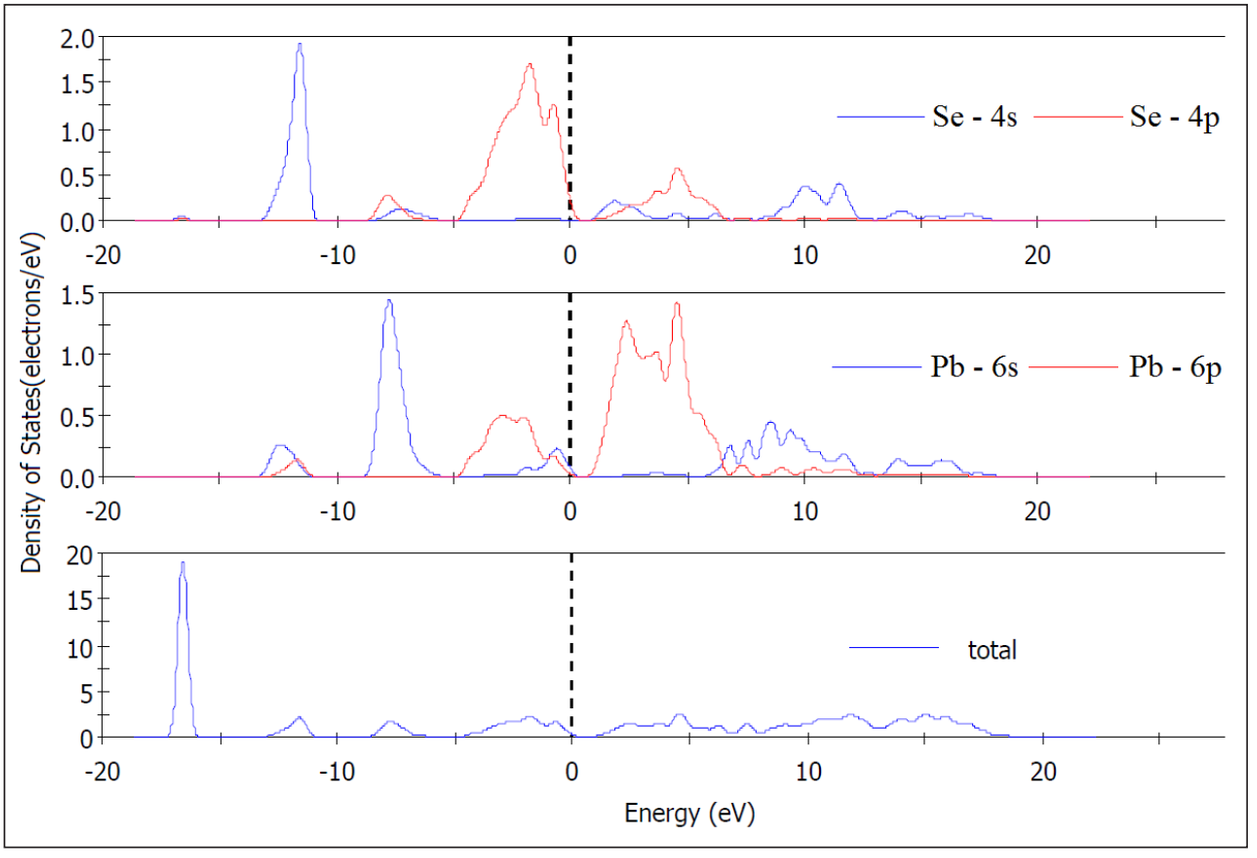

Figure 4: *Total and partial densities of states for PbSe. The position of the Fermi level is set at 0.0 eV.*

by the specific surface energy and Gibbs free energy, which depends on reaction conditions. The sphere-like particles can act as nuclei particles to allow growing spherical morphologies due to the ability of oleylamine surfactant to prevent the nanoparticles from approaching the surface because of its steric stabilization effect. The reactions summarized as follows:

$NaBH_4 + H_2O \rightarrow H_2 + NaBO_2$ (1)

$Se + H_2 \rightarrow Se^{2-}$ (2)

Pb^{2+} + EDTA (or oleylamine) → Pb^{2+}-EDTA(complex) (or Pb^{2+}-oleylamine) (3)

Pb^{2+}-EDTA(complex) (or oleylamine) + Se^{2-} → PbSe + EDTA (or oleylamine) (4)

2.3. Band structure

The calculated band structure of the compounds along high symmetry points of the first Brillouin zone has plotted in Figure 3, where the labeled *k* points are presented as W (0.500, 0.250, 0.750), L (0.500, 0. 500, 0.500), G (0.000, 0.000, 0.000), X (0.500, 0.000, 0. 500), K (0.375, 0.375, 0.750). It is found that the top of the valence bands (VBs) has a small dispersion, whereas the bottom of the conduction bands (CBs) has a large dispersion. The lowest energy (0.500 eV) of the conduction bands (CBs) is localized at the L point, and the highest energy (0.00 eV) of VBs is localized at the L point too. So, the material has direct band gap.

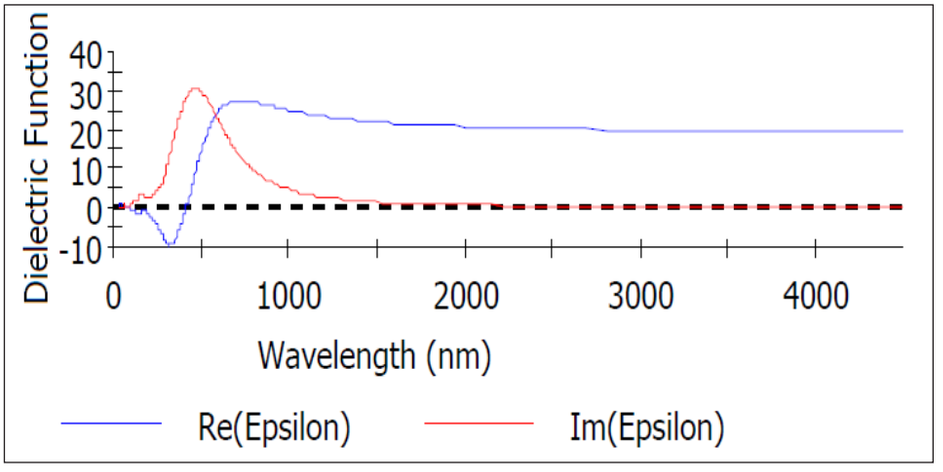

Figure 5: *Dielectric functions of PbSe.*

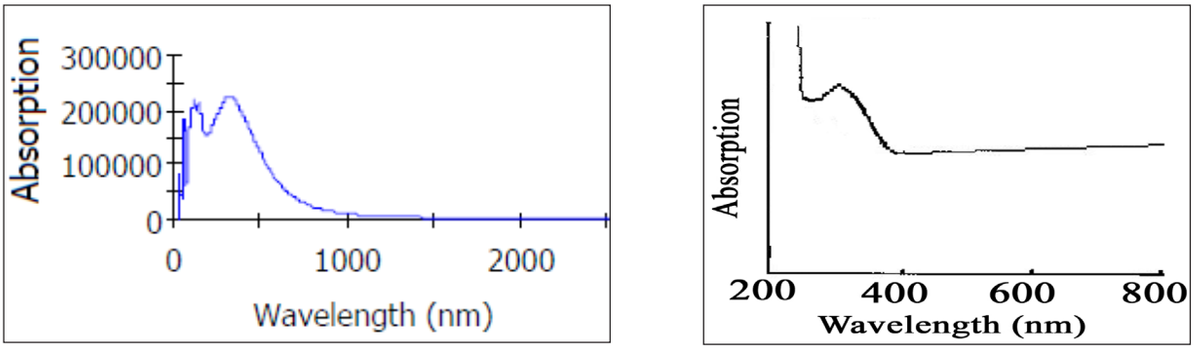

Figure 6: *Calculated (left) and experimental (synthesized at 24h with EDTA) (right) absorption spectra of PbSe nanomaterials.*

2.4. Electronic structure

The total density of states (TDOS) and partial densities of states (PDOS) for PbS are shown in Figure 4. three regions are evident in the valence band of the PbSe, the first one, approximately from -13 eV to -11 eV, has significant contributions from Se-4s state; however, small contributions from Pb-6s and 6p states can be observed at these energy intervals. The second one, from -8 eV to -6 eV, has major contribution from Pb-6s with small contribution of Se-4s and 4p states and the third region are from 5 eV to the Fermi level (0.0 eV) attributed to Se-4p and Pb-6s and 6p. The conduction bands between 0.5 eV and 17 eV come from Pb-6s, 6p states and Se-4s, 4p states. Such a splitting characteristic of valence bands reflects different bonding behaviors. The first and second parts are due to the weak interaction between Se and Pb orbits while the third part indicates the covalent bonds between Se-4p and Pb-6s and 6p orbits.

2.5. Optical properties

The optical properties of a solid materials are usually described by the complex dielectric function $\varepsilon(\omega) = \varepsilon_1(\omega) + i\varepsilon_2(\omega)$, which characterizes the linear response of the material to an electromagnetic radiation, and therefore governs the propagation behavior of radiation in a medium. The imaginary part of the dielectric function $\varepsilon_2(\omega)$ represents the optical absorption in the crystal, which can be calculated from the momentum matrix elements between the occupied and unoccupied states, and the real part $\varepsilon_1(\omega)$ is evaluated from the imaginary part $\varepsilon_2(\omega)$ by the Kramers-Kronig transformation. Based on the electronic structure, the dielectric functions of PbSe were calculated. The $\varepsilon_1(\omega)$ and $\varepsilon_2(\omega)$ as a function of the photon energy are shown in figure 5.

The imaginary part of $\varepsilon(\omega)$ in PbSe has two bands located at 4.96 eV and 2.48 eV. These bands mainly correspond to the transition from Se-4p states (VBs) to the empty Pb-6p states (CBs) above the Fermi level. For the real part $\varepsilon_1(\omega)$ of the dielectric function $\varepsilon(\omega)$, the most important quantity is the zero frequency limit $\varepsilon_1(0)$, which is the electronic part of the static dielectric constant and strongly depends on the band gap. A smaller energy gap yields a larger $\varepsilon_1(0)$ value. This could be explained on the basis of the Penn model ($\varepsilon_1(0) \approx 1 + (h\omega_P / E_g)^2$) [35]. We can determine E_g from this expression by using the values of $\varepsilon_1(0)$ and the plasma energy $h\omega_P$. The calculated static dielectric constants $\varepsilon_1(0)$ is 0 eV .

The calculated and experimental results on the absorption spectra were shown in Figure 6. According to the calculated absorption spectrum, the absorption edges are located at 125 nm and 375 nm for PbSe. Experimental UV-Vis absorption spectrum of the Synthesized PbSe nano-cubes at room temperature (Figure 6) is according to calculated spectrum. The position of the observed peaks shows that these bands correspond mainly to the transition from Se-*4p* states (VBs) to the empty Pb-*6p* states (CBs) above the Fermi level (Figure 4).

3. EXPERIMENTAL

3.1. Preparation

The synthetic procedure is as follows: 0.580 g lead nitrate ($Pb(NO_3)_2$), 0.6 g EDTA (ethylenediamine triacetic acid) 0.2 g Se and 0.5 g NaOH was dissolved in 75mL deionized water under stirring in a Teflon-lined stainless-steel autoclave of 100mL capacity. Then 0.554 g $NaBH_4$ was added into the above solution under stirring for another 10 min. The Teflon-lined autoclave was tightly sealed and maintained for 24 h, 48h or 96h at 180°C, respectively. The autoclave was then allowed to cool to room temperature naturally. For synthesis of spherical PbSe, oleylamine was used instead of EDTA. Black precipitates was collected by centrifugation and washed several times with distilled water and pure ethanol, respectively. In the case of spherical, the sample was dried in vacuum at 60°C for 6 h, finally.

3.2. Product characterizations

The crystal structure and phase purity of PbSe nanoparticles have been characterized by powder X-ray diffraction (PXRD) on a Siemens D500 using Cu-k_α radiation (λ=1.541Å). UV–Vis absorption spectra were recorded employing a PG instruments

Ltd T70 UV/Vis spectrophotometer. Surface morphology and distribution of the particles have been studied via a Philips model XL30 scanning electron microscope (SEM).

3.3. Computational details

The electronic band structures along with the DOS of the compounds are calculated by density functional theory (DFT) using one of the three non-local gradient-corrected exchange-correlation functional (GGA-PBE). Calculations were performed with the CASTEP code [31, 32], which uses a plane wave basis set for the valence electrons and norm-conserving pseudopotential (NCP) [33] for the core electrons. The number of plane waves included in the basis was determined by cut-off energy Ec of 500.0 eV The summation over the Brillouin zone was carried out with a *k*-point sampling using a Monkhorst-Pack grid [34] with parameters of 5×5×5. The parameters used in the calculations and convergence criteria were set by the default values of the CASTEP code, e.g., reciprocal space pseudopotentials representations, eigen-energy convergence tolerance of 1×10^{-6} eV, Gaussian smearing scheme with the smearing width of 0.1 eV, and Fermi energy convergence tolerance of 1×10^{-7} eV.

4. ACKNOWLEDGMENTS

This study has been supported by the Council of the University of Tabriz and University of Kharazmi.

REFERENCES

1. I. N. Chao, P.J. McCann, W. L. Yuan, E. A. Rear, S. Yuan, Thin. Solid Films, Vol. 323, (1998), p. 126.
2. T. J. Liptay, R. J. Ram, App. Phys. Lett. Vol. 89, (2006), p. 223132.
3. S. Prabahar, N. Suryanarayanan, K. Rajasekar, S. Srikanth, D. Kathirvel, Chalcogenide Lett. Vol. 6, (2009), pp. 399–402.
4. R. Y. Wang, J. P. Feser, J. S. Lee, D. V. Talapin, R. Segalman, A. Majumdar, Nano Lett. Vol. 8, (2008), pp. 2283-2288.
5. R. A. Orozco, M. Sotelo-Lerma, R. Ramirez-Bon, M. A. Quevedo-Lopez, O. Mendoza-Gonzalez, O. Zelaya-Angel, Thin Solid Films, Vol. 587, (1999), pp. 343–344.
6. I. Pop, C. Nascu, V. Ionescu, E. Indrea, I. Bratu, Thin Solid Films, Vol. 307, (1997), p. 240.
7. H. Zogg, A. Fach, J. John, J. Masek, P. Muller, C. Paglino, W. Butter, Opt. Eng. Vol. 33, (1994), p.1440.
8. S. Chatterjee, U. Pal, Opt. Eng. Vol. 32, (1993), p. 2923.
9. M. Kowshik, W. Vogel, J. Urban, S. K. Kulkarni, K. M. Paknikar, Adv. Mater. Vol. 14, (2002), p. 815.
10. J. J. Zhun, H. Wang, S. Xu, H. Y. Chen, Langmuir, Vol. 18, (2002), p. 3306.
11. Z. Li, C. Wu, Y.Y. Liu, T.B. Liu, Z. Jiao, M. H. Wu, Bull. Mater. Sci. Vol. 31, (2008), p. 825.
12. J. U. Chang, C. Liu, J. Heo, J. Non-Cryst. Solids, Vol. 355, (2009), p. 1897.
13. L. Bakueva, I. Gorelikov, S. Musikhin, X. S. Zhao, E. H. Sargent, E. Kumacheva, Adv. Mater. Vol. 16, (2004), p. 926.
14. J. J. Zhu, S. T. Aruna, Y. R. Koltypin, A. Gedanken, Chem. Mater. Vol. 12, (2000), p. 143.
15. X. Q. Wang, G. C. Xi, Y. K. Liu, Y. T. Qian, Cryst. Growth. Des. Vol. 8, (2008), p. 1406.
16. K. L. Hull, J. W. Grebinski, T. H. Kosel, M. Kuno, Chem. Mater. Vol. 17, (2005), p. 4416.
17. K. Cho, D. V. Talapin, W. Gaschler, C. B. Murray, J. Am. Chem. Soc. Vol. 127, (2005), p. 7140.
18. F. Melissa, A. I. Hochbaum, J. Goldberger, M. Zhang, P. D. Yang, Adv. Mater. Vol. 19, (2007), p. 3047.
19. M. J. Bierman, Y. K. Albert Lau, J. Song, Nano Lett. Vol. 7, (2007), p. 2907.
20. U. Kumar, S. N. Sharma, S. Singh, M. Kar, V. N. Singh, B. R. Mehta, R. Kakkar, Mater. Chem. Phys. Vol. 113, (2009), p. 107.
21. K. T. Yong, Y. Sahoo, K. R. Choudhury, M. T. Swihart, J.R. Minter, P. N. Prasad, Nano Lett. Vol. 6, (2006), p. 709.
22. J. Xu, J. P. Ge, Y. D. Li, J. Phys. Chem. B, Vol. 110, (2006), p. 2497.

23. A. J. Houtepen, R. Koole, D. Vanmaekelbergh, J. Meeldijk, S. G. Hickey, J. Am. Chem. Soc. Vol. 128, (2006), p. 6792.

24. R. R. Reddy, K. R. Gopal, K. Narasimhulu, L. S. S. Reddy, K. R. Kumar, G. Balakrishnaiah, M. R. Kumar, J. Alloys Compd. Vol. 473, (2009), p. 28.

25. G. Martinez, M. Schluter, M. L. Cohen, Phys. Rev. B, Vol. 11, (1975), p. 651.

26. K. M. Rabe , J. D. Joannopoulos, Phys. Rev. B, Vol. 32, (1985), p. 2302.

27. S. H. Wie, A. Zunger, Phys. Rev. B, Vol. 55 (1997), p. 13605.

28. E. A. Albanesi, C. M. I. Okoye, C. O. Rodriguez, E. L. Peltzer y Blanca, A. G. Petukhov, Phys. Rev. B, Vol. 61, (2000), p. 16589.

29. M. Lach-hab, D. A. Papaconstantipoulos, M. J. Mehl, J. Phys. Chem. Solids, Vol. 63, (2002), p. 833.

30. K. Hummer, A. Grüneis, G. Kresse, Phys. Rev. B, Vol. 75, (2007), p. 195211.

31. S. J. Clark, M. D. Segall, C. J. Pickard, P. J. Hasnip, M. J. Probert, K. Refson, M. C. Payne, Materials Studio CASTEP, version 5.0, Accelrys: San Diego, CA, (2009).

32. S. J. Clark, M. D. Segall, C. J. Pickard, P. J. Hasnip, M. J. Probert, K. Refson, M.C. Payne, Z. Kristallogr. Vol. 220, (2005), pp. 567-570.

33. D. R. Hamann, M. Schluter, C. Chiang, Phys. Rev. Lett. Vol. 43, (1979), pp. 1494-1497.

34. H. J. Monkhorst, J. Furthmuller, Phys. Rev. B, Vol. 13, (1976), 13, pp. 5188-5192.

35. K. F. Hesse, Acta Cryst. B, Vol. 33, (1977), p. 901.